Self-Assembled Block Copolymer Thin Films as Water Filtration Membranes

William A. Phillip,[†] Brandon O'Neill,[†] Marc Rodwogin,[‡] Marc A. Hillmyer,[‡] and E. L. Cussler*,[†]

Department of Chemical Engineering and Materials Science and Department of Chemistry, University of Minnesota, Minneapolis, Minnesota 55455

ABSTRACT Nanoporous membranes containing monodisperse pores of 24 nm diameter are fabricated using poly(styrene-*b*-lactide) block copolymers to template the pore structure. A 4 μm thin film of the block copolymer is cast onto a microporous membrane that provides mechanical reinforcement; by casting the copolymer film from the appropriate solvents and controlling the solvent evaporation rate, greater than 100 cm^2 of a thin film with polylactide cylinders oriented perpendicular to the thin dimension is produced. Exposing the composite membrane to a dilute aqueous base selectively etches the polylactide block, producing the porous structure. The ability of these pores to reject dissolved poly(ethylene oxide) molecules of varying molecular weight matches existing theories for transport through small pores.

KEYWORDS: block copolymer • poly(styrene-*b*-lactide) • perpendicular orientation • nanoporous membrane • filtration

INTRODUCTION

Copolymers are promising materials for making improved ultrafiltration (UF) membranes. The addition of graft copolymers to the casting dopes of membranes made by traditional phase-inversion techniques has dramatically increased their ability to resist fouling (1, 2). The self-assembly of block polymers can produce membranes with narrow pore-size distributions and high porosities, an advantage over current UF membranes with polydisperse pore sizes (3−9). Nanoporous membranes templated by self-assembled block polymers produce sharper molecular weight cut-offs (MWCOs) than current phase-inversion membranes. Films containing a bicontinuous porous network have been prepared using block polymers. Because these pores are isotropic and percolate through the membrane, their alignment is not an issue (6, 9). However, these bicontinuous-based microstructures contain some double-conical structures, which may contribute to membrane fouling.

We are continuing our pursuit of nanoporous membranes templated by the cylindrical block polymer morphology. Such monodispersed pores should result in superior selectivity, the high void fraction (ca. 25%) should allow for high fluxes, and the smooth surface of block-polymer-derived membranes suggests that fouling will be reduced (10−12). However, to be effective, these cylindrical pores must be perpendicular to the membrane surface.

Earlier studies have aligned cylinder-forming block copolymers using shear forces (5, 13), controlled substrate−polymer interactions (3, 4), and solvent evaporation during a phase-inversion process (8). Shear aligning the cylinders typically produces samples that are millimeters in thickness, too thick for commercial UF operations. The methods that control substrate−polymer interactions begin by coating a block polymer thin film onto a solid substrate, subsequently floating the fragile thin film off of the substrate, and picking it up with a porous support. This is difficult for large-scale membrane preparation. The phase-inversion technique can be used to prepare a 500 nm self-assembled selective layer. However, because the support layer in this membrane is also made from the same block polymer, the resulting membranes will be expensive.

The composite membranes produced in this work suggest a way to reduce the cost of block-polymer-templated UF membranes while still taking advantage of their significant potential. These membranes are made using a robust, inexpensive microporous membrane as a mechanical support. A 500−1000 nm thin selective layer is cast onto this support, allowing the separation and support functions to be optimized independently (14−16). The composite membranes produced here used controlled evaporation to align the block copolymer sample with perpendicularly oriented cylinders in a single step. The block polymer used is poly(styrene-*b*-lactide) (PS−PLA), where the polylactide (PLA) block forms the cylinders (13, 17, 18). After casting, the composite membrane is washed with a dilute base to selectively etch the PLA block. This process yields a UF membrane with a porous selective layer containing monodisperse pores, templated by block polymer self-assembly.

In the sections below, the casting, alignment, and selective etching steps are discussed. The various casting conditions suggest how control of the solvent evaporation rate can lead to a perpendicular orientation in some systems but not others. The practical value of these membranes is explored

* To whom correspondence should be addressed. E-mail: cussl001@umn.edu.
Received for review December 12, 2009 and accepted February 1, 2010
[†] Department of Chemical Engineering and Materials Science.
[‡] Department of Chemistry.
DOI: 10.1021/am900882t

Table 1. Copolymer Properties for Each Sample

sample name	PS M_n[a] (kg mol^{-1})	PLA M_n[b] (kg mol^{-1})	PDI[c]	f_{PLA}[d]
SL(27-11)	26.6	11.0	1.05	0.26
SL(27-12)	26.6	12.1	1.05	0.28
SL(27-13)	26.6	13.3	1.05	0.30
SL(27-15)	26.6	14.6	1.06	0.32
SL(42-15)	41.6	15.4	1.05	0.27
SL(52-19)	52.0	19.4	1.05	0.27
SL(71-24)	70.5	24.3	1.09	0.26

[a] Molecular weight of the styrene block. [b] Molecular weight of the lactide block. [c] Polydispersity index. [d] Volume fraction of lactide (f_{PLA}) in the sample.

by measuring the pure water fluxes and demonstrating selectivity using a series of narrow molecular weight distribution poly(ethylene oxide) samples. While the results show that the promise of block-polymer-templated thin films is real, we identify the challenges that must be overcome to realize their full potential.

EXPERIMENTAL SECTION

Membrane Preparation. A series of asymmetric poly(styrene-*b*-polylactide) (PS−PLA) block copolymers were used as templates for the nanoporous membranes fabricated in this work. The PS−PLA copolymer samples were prepared using a combination of anionic and controlled ring-opening polymerization protocols. Detailed descriptions of the PS−PLA synthesis are given elsewhere (13, 17, 18). The overall polymer molecular weight and volume fraction were determined using ^{1}H NMR spectroscopy, and the polydispersity index was determined using size-exclusion chromatography. Table 1 summarizes the properties of the different samples. Note that the first four samples have near constant M_n and increasing values of f_{PLA}, while the last three have increasing M_n but near constant f_{PLA}. The first four samples were synthesized from the same PS block, but the molecular weights of the PLA blocks were slightly different; this changed f_{PLA} without dramatically impacting the dynamic properties of the copolymer. Small-angle X-ray scattering (SAXS) was used to confirm that all of the samples formed a cylindrical morphology.

The general procedures for preparing a membrane were identical in each case, but the copolymer and solvent were varied. The casting procedure started by placing a clean dust-free glass plate on a level surface inside a fume hood. A 5 cm × 5 cm square of the microporous support membrane (Biomax 1000 kDa, Millipore Co., Cambridge, MA) was cut from a larger sheet and floated on top of water in a Petri dish for 30 s, allowing the water to wick into the pores. Once the membrane pores were wet, the initially opaque white membrane became slightly translucent. The support was then removed from the Petri dish, gently shaken to remove excess water, and placed on top of the glass plate.

The membrane casting solution, prepared 2 h prior to membrane fabrication, consisted of 8 wt % polymer dissolved in a solvent. The time that it took for the solution to appear homogeneous depended on the solvent quality and polymer molecular weight but never took longer than 2 h. With the wetted support membrane in place, 1 mL of a casting solution was dispensed onto the glass plate and then drawn across the support membrane using a wire-wound rod. After the solvent was allowed to evaporate for 30 s, the glass plate was moved to a 60 °C oven, where it was kept for 20 min. The oven temperature was reduced to 30 °C, and the membrane was dried overnight.

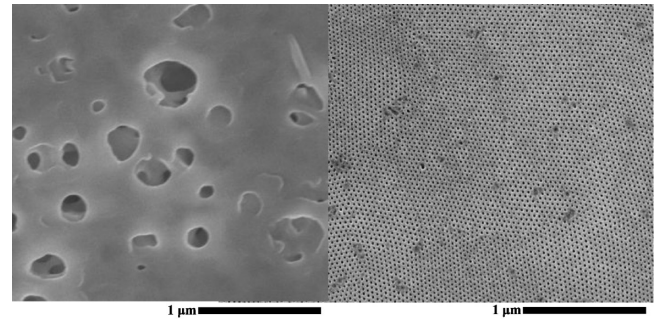

FIGURE 1. Selective copolymer layer coated onto a microporous support membrane. The image on the left shows the bare poly(ether sulfone) support, and the image on the right shows the pores of the copolymer-templated thin selective layer.

The solvents used for the casting solution were all water-immiscible; therefore, the casting solution was excluded from the water-filled pores of the support. Once the solvent had evaporated, a thin block polymer film was left sitting on top of the microporous support layer, yielding the desired two-layer composite structure. Early attempts to make membranes were plagued by small cracks in the copolymer layer, which we attributed to residual stresses. By drying of the film at 60 °C, the plasticized polymer remains above its glass transition temperature longer and the residual stresses are allowed to relax. Cooling the samples slowly by reducing the oven temperature to 30 °C and leaving them overnight allowed the stresses that arise from the difference in the coefficients of thermal expansion between the copolymer and support layer to be minimized. Once dried, the composite membrane was exposed to ultraviolet (UV) light (λ = 254 nm) for 20 min to improve the adhesion between the copolymer and microporous layers (19). This step was included because some films would delaminate during the etching process. The UV exposure both prevents this and cross-links the polystyrene (PS) block (20, 21). Following this procedure, we could fabricate crack-free membranes with areas greater than 100 cm^2.

The samples were then prepared either for inspection by scanning electron microscopy (SEM) or for liquid-flow and UF experiments. Preparing a sample for SEM consisted of cutting a 1 cm × 1 cm piece from the larger sample, etching the PLA block by submerging the sample in a 0.5 M 60:40 (v/v) methanol/water and NaOH solution for 1 h, and then transferring the sample to base-free 60:40 (v/v) methanol/water for 30 min to rinse the membrane. The samples were dried overnight at room temperature and then coated with a 2−3 nm layer of gold prior to SEM to help prevent sample charging. Figure 1 shows SEM images of the top surface of the support membrane (left) and the composite membrane after the casting procedure (right).

Sample preparation for transport measurements was more involved because the membranes were first checked for defects. A 2.5 cm diameter sample was punched out of the 5 cm × 5 cm square using a hole punch. This disk was placed in an Amicon 8010 stirred cell (Millipore Co., Cambridge, MA) and secured using a silicone O-ring. The cell was filled with 60:40 (v/v) methanol/water, and a pressure drop of 25 psig was applied across the membrane using N_2 gas. If no flow was observed over a 3 h period, the membrane was considered defect-free and an etching solution was loaded into the cell. The etching solution was left in the cell overnight to ensure that all of the PLA was fully degraded. Water was then used to flush the membrane for 2 h at a pressure drop of 25 psig, rinsing away the etching solution. Because the etching solution contains methanol, the membranes are wet during the etching step and no prewetting steps are required. This preparation method minimizes the handling of the sample and helps to prevent the selective copolymer layer from being damaged.

Table 2. Molecular Weights and Characteristic Sizes of the PEO Solutes

PEO sample M_n (kg mol^{-1})	PDI[a]	$R_H(D)(22)$ (nm)	$R_H([\eta])(23)$ (nm)
14.0	1.04	3.4	4.0
23.5	1.03	4.5	5.4
35.0	1.06	5.7	6.8
59.0	1.02	7.8	9.0
100.0	n/a	10.6	12.1

[a] As reported by the manufacturer.

UF Experiments. Liquid permeation experiments were performed by forcing pure water across the membrane, using N_2 gas (UHP N_2, Airgas, Radnor Township, PA). The permeating water was collected in a glass vial, and its mass was measured (Mettler-Toledo, Inc., Columbus, OH) every 5 min over 1 h. Flow rate measurements were performed three times at each pressure drop to check reproducibility. The observed flux was not a function of time, indicating that little to no compaction occurred.

A solution of a poly(ethylene oxide) (PEO) sample (Polymer Source Inc., Montreal, Quebec, Canada) with a narrow molecular weight distribution, dissolved at a concentration of 1.5 g L^{-1}, was used to challenge the nanoporous membrane. Single-solute experiments were performed using five different PEO molecular weights (14.0 23.0, 34.5, 59.0, and 100.0 kg mol^{-1}), selected because the molecules have hydrodynamic radii in the size range of the pores (Table 2). The hydrodynamic radii were calculated using published data of tracer diffusion coefficients (22) and intrinsic viscosities (23), and the concentrations of PEO were determined by evaluating the total organic carbon in the permeate, as we described in our previous work (6).

RESULTS

The experimental results are clearly discussed as three topics. First, we will discuss our efforts to prepare large areas of membrane with oriented pores. This is accomplished by selecting particular copolymers and solvents and then controlling the solvent evaporation rate. Second, we report liquid-water-flow experiments, which measure the pure water hydraulic permeability. We can compare our measured values with values predicted by fluid mechanics and with representative values for other UF membranes with similar MWCOs. Third, we probe the practical value of the new block-polymer-templated composite membranes by measuring their ability to reject dissolved solutes.

Membrane Fabrication. Experiments attempting to orient the PLA cylinders begin by exploring the effects of the solvent evaporation rate. For fast evaporation, the cast film was left exposed to the ambient atmosphere after drawing the polymer solution across the microporous support. Drying took about 5 min. For slower evaporation, the sample was covered with a Petri dish directly after drawing the solution across the support. In this case, drying took about 2 h. Figure 2 shows representative SEM images of the free surface for two samples of SL(27-11) cast from toluene. Fast evaporation yields the desired hexagonally packed perpendicular cylindrical structure at the surface of the membrane, while slow evaporation produces a parallel cylinderical structure at the surface of the membrane. This suggests that the perpendicular cylinders are a kinetically trapped nonequilibrium structure (24–27). This argument is strengthened by

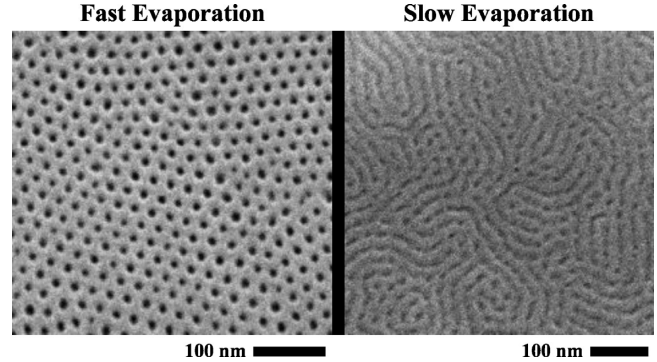

FIGURE 2. Fast evaporation needed for perpendicularly oriented cylinders. Evaporating toluene quickly kinetically traps the cylinders in a nonequilibrium perpendicular structure, while slow evaporation produces a parallel orientation.

Table 3. Solubility Parameters for the Solvents and Polymers

solvent	$\bar{V}_1$ (cm^3 mol^{-1})	δ_v (MPa$^{1/2}$)	δ_h (MPa$^{1/2}$)
chlorobenzene	101.41	19.1	2.0
chloroform	80.66	18.1	5.7
toluene	105.91	18.1	2.1
1,1,2-tricholoroethane	101.06	17.5	2.1
polymer	δ_v (MPa$^{1/2}$)		δ_h (MPa$^{1/2}$)
PS	19.0		10.1
PLA	19.0		5.0

SEM images of a fast-evaporation sample that has been dried and then annealed under toluene for 30 min. The resulting images are virtually identical with the images from the slow-evaporation protocol, indicating that with enough time and mobility the polymer chains will rearrange to the thermodynamically favored parallel orientation (19).

Solvent selectivity can also influence the cylinder orientation (24, 27). To explore this, we cast membranes under fast-evaporation conditions using the SL(27-11) copolymer sample and a variety of solvents. Several properties of the selected casting solvents are given in Table 3.

The first column gives the solvent molar volume, and the next two columns give the dispersive and polar contributions to the solvent and polymer solubility parameters (28).

The solubility parameters in Table 3 were used to calculate the polymer–solvent interaction parameter χ_{1-2}

$$\chi_{1-2} = \frac{\bar{V}_1}{RT}[(\delta_{1,v} - \delta_{2,v})^2 + (\delta_{1,h} - \delta_{2,h})^2] \qquad (1)$$

where $\bar{V}_1$ is the solvent molar volume, R is the gas constant, T is the drying temperature of 65 °C, $(\delta_{1,v} - \delta_{2,v})$ is the difference between the volume dependent contribution of the solvent and polymer solubility parameters, and $(\delta_{1,h} - \delta_{2,h})$ is the difference between the hydrogen bonding dependent contributions. Solvent selectivity was assessed using the results of these calculations (Table 4) (19).

All four solvents favor PS but to varying degrees. The three solvents classified as PS-selective—chlorobenzene, toluene, and 1,1,2-trichloroethane—are strongly selective for

Table 4. χ Interaction Parameters between the Solvents and Polymers

solvent	$\chi_{PS-solvent}$	$\chi_{PLA-solvent}$
chlorobenzene	0.33	2.37
chloroform	0.04	0.58
toluene	0.35	2.45
1,1,2-tricholoroethane	0.38	2.38

PS. This is reflected in the small $\chi_{PS-solvent}$ and the large $\chi_{PLA-solvent}$ for these three solvents. On the other hand, chloroform is only a slightly selective solvent because of the much smaller difference between $\chi_{PS-solvent}$ and $\chi_{PLA-solvent}$ and so is referred to as a neutral solvent. The PS-selective solvents resulted in perpendicular cylinders, while membranes cast from the neutral solvent chloroform had a mixture of perpendicular and parallel orientations. The difference between these two cases can be seen in Figure 3.

Another variable found to affect the orientation of the cylinders is the block copolymer composition (29). To investigate this variable in our system, we explored cylinder-forming samples with nearly the same overall molecular weight but with PLA volume fractions ranging from 0.26 to 0.32. Changing the PLA fraction from 0.26 to 0.28 results in a switch in the cylinder orientation from perpendicular to parallel when cast using a toluene solution. Similarly, the change from perpendicular to parallel orientation occurred in trichloroethane and chlorobenzene but at different PLA volume fractions (0.30 and 0.32, respectively). Similar results have been documented by others working with different systems (29).

The final copolymer property explored in this work is the effect of the overall copolymer molecular weight. Copolymer samples with PLA volume fractions between 0.25 and 0.27 but with different molecular weights were cast as membranes using trichloroethane and the fast-evaporation protocol. While samples SL(27-11) and SL(42-15) produce hexagonally packed perpendicular cylinders, sample SL(52-19) forms what appears to be a dimpled structure, as shown in Figure 4. The sample does look as if it has a hexagonally packed surface structure with some open pores, but sample SL(71-24) has a more dimpled structure with fewer open pores.

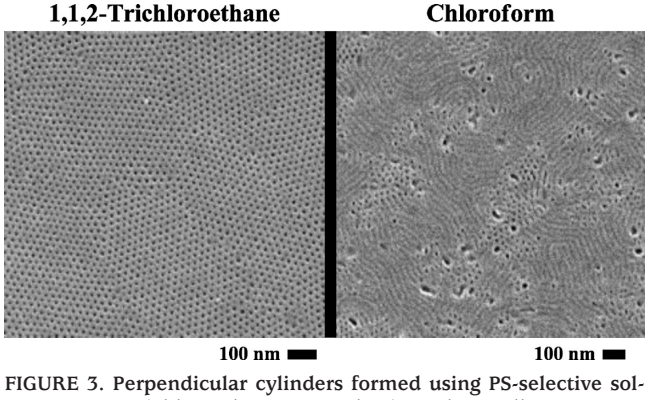

FIGURE 3. Perpendicular cylinders formed using PS-selective solvents. 1,1,2-Trichloroethane a PS-selective solvent allows perpendicular cylinders to be obtained, while a mixed-orientation sample is produced when casting from the neutral solvent chloroform.

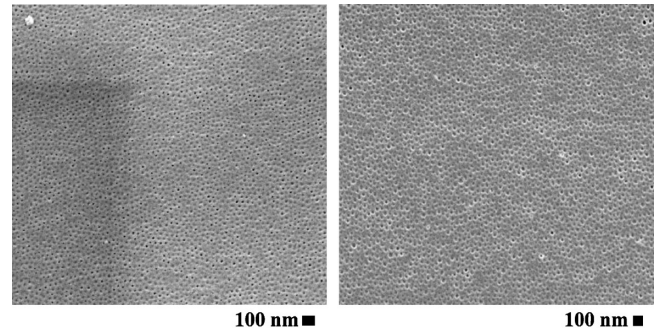

FIGURE 4. Higher molecular weight samples that form "pits" not pores. A small fraction of the cylinders form pores for the membrane cast from the SL(52-19) sample, shown on the left. The number of pores formed for the membrane cast from the SL(71-24) sample, on the right, is even smaller, with most of the cylinders forming "pits".

Water-Flow Experiments. We developed a technique to reproducibly prepare 100 cm^2 membrane areas that could be used for characterizing the transport properties of block copolymer membranes. A digital micrometer was used to measure the thickness of these membranes. Direct measurement of the copolymer layer thickness was possible for films that had delaminated from the support layer; five measurements were taken at different points and averaged. The selective layer thicknesses of UV-treated membranes were determined by measuring the support layer thickness and the composite membrane thickness and then taking the difference of the two values as the selective layer thickness. Within experimental error, the two methods gave the same average thickness of 4 $\pm$ 2 μm for the selective layer prepared from SL(42-15). These membranes are thicker than commercial composite membranes, and attempts to make thinner membranes were unsuccessful because of limitations of the hand-casting membrane techniques.

Because the pores are small, the fluid velocity for a single pore $\langle v \rangle$ is laminar and is described by the Hagen–Poiseuille law (30, 31)

$$\langle v \rangle = \frac{d^2 \Delta p}{32 \mu l} \tag{2}$$

where Δp is the pressure drop across a membrane of thickness l with pore diameter d and η is the liquid viscosity. For a porous solid, the superficial velocity $\bar{v}$ is more useful:

$$\bar{v} = \frac{\varepsilon}{\tau} \frac{d^2 \Delta p}{32 \mu l} \tag{3}$$

where ε is the void fraction and τ is the tortuosity. The void fraction accounts for the experimental measurements being based on the total projected area of the membrane, not on the cross-sectional area of the pores. The tortuosity accounts for both variations in the shape of the pore cross section and the additional distance required for a molecule to travel (32).

To illustrate the effects involved, we report liquid convection and solute rejection for a membrane made by casting

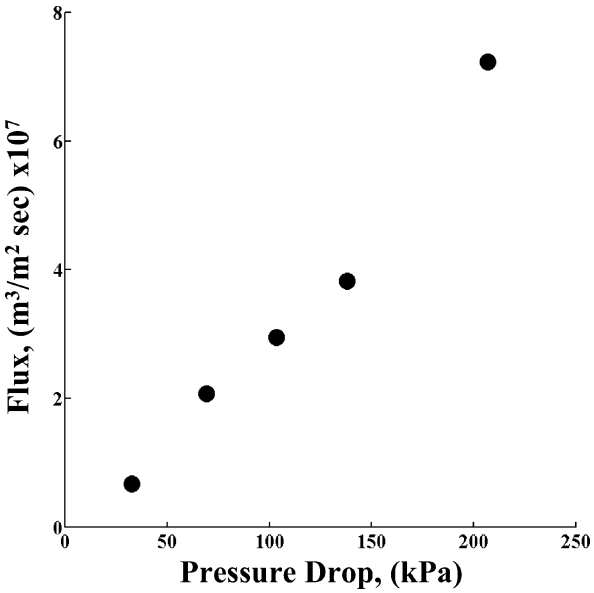

FIGURE 5. Pure water flux that is proportional to the pressure drop. Experimentally observed fluxes for sample SL(42-15) vary linearly with respect to the pressure drop, as predicted by eq 2.

the sample SL(42-15) copolymer from the solvent 1,1,2-trichloroethane. The flux ($m^3\ m^{-2}\ s^{-1}$) is plotted in Figure 5 versus the pressure drop (kPa). The linear relationship expected from eq 3 is observed. From linear regression, the pure water permeability of the composite membrane is determined to be 1.15 L m^{-2} h^{-1} bar^{-1}.

This experimentally determined permeability should be compared with several characteristic values. First, to ensure that the nanoporous polymer layer is the dominant resistance to mass transfer, we determined a permeability of 3060 LHM bar^{-1} for the microporous support membrane. This value is over nearly 3000 times that of the composite membrane. Thus, flow through our nanopores provides the dominant resistance (14, 30, 31). Second, we compare our measured hydraulic permeability to that predicted by eq 3. Using a pore diameter of 24.2 nm (SAXS), a void fraction of 0.27 (from the PLA volume fraction in Table 1), a tortuosity of 1 (the value for perfectly perpendicular pores), and a film thickness of 4 μm (as determined above), we predicted a permeability of 450 L m^{-2} h^{-1} bar^{-1}, a value nearly 400 times the experimental permeability.

The structure of the composite membrane suggests three possible reasons for this observed difference. First, if we overlay the image on the right of Figure 1 onto the image from the left of Figure 1, we can see that the support membrane may block a large number of nanopores, reducing the actual void fraction from 0.27 to about 0.03. This would reduce the predicted permeability to 50 L m^{-2} h^{-1} bar^{-1}, still much greater than that observed. Second, the right circular cylinders may not span the entire membrane thickness. To test this hypothesis, O_2 plasma reactive ion etching was used to remove 100 nm of the copolymer layer from the top. As Figure 6a shows, the perpendicular cylinder orientation becomes a mixed perpendicular and parallel orientation in the bulk. This transition occurs approximately 100 nm into the film. This apparent tortuosity would account

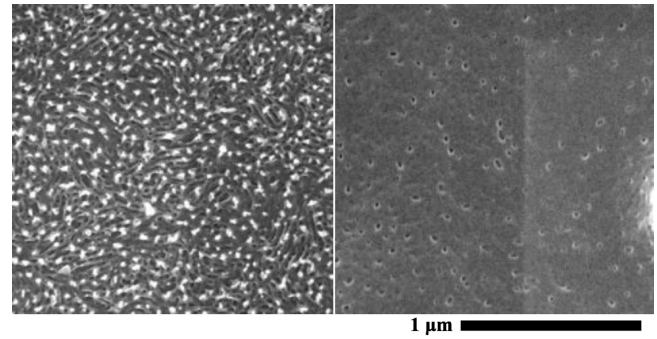

FIGURE 6. Flaws in the membrane that reduce its hydraulic permeability. The SEM image on the left shows that the cylinders switch from a perpendicular to a mixed orientation 100 nm into the film. An image on the right, of the membrane backside, shows that not all of the pores span the membrane thickness. These flaws explain the low flow rates observed.

for another reduction in the flux. Assuming a tortuosity of 2, the predicted flux would decrease to 25 L m^{-2} h^{-1} bar^{-1}. Third, a film that delaminated during the etching step was inverted so that the bottom side morphology could be observed. An SEM image of this bottom surface, given in Figure 6b, shows that only a small fraction of the pores, less than 10%, span the entire membrane thickness. Likewise, this would lead to a large reduction in the flux.

Rejection Experiments. While the factors discussed in the previous paragraph reduce the fluxes, neither the mixed morphology nor the reduced void fraction should compromise the ability of the membrane to selectively reject dissolved solutes. The ability of the membrane to perform such a separation is described by the sieving coefficient S_a (33), defined as the concentration in the permeate divided by that at the upstream membrane surface. The ratio of the permeate velocity, $\bar{v}$, to the mass-transfer coefficient of the solute in the bulk solution k is small, indicating that the solute concentration at the membrane surface and in the bulk feed are nearly equal. Using the correlation given by Zeman and Zydney for a stirred cell geometry (34) at a stirring speed of 400 rpm, we calculate a mass-transfer coefficient of 1.1×10^{-5} m s^{-1} for the 59 kDa PEO sample. This mass-transfer coefficient and the filtrate flux at 150 kPa give a value for $\bar{v}/k$ of 0.05. Thus, we are measuring the sieving coefficient of the membrane in our experiments, not an experimental artifact that arises from concentration polarization.

These UF experiments made using a membrane fabricated from copolymer sample SL(42-15) are summarized in Figure 7 as the percent rejected [$(1 - S_a) \times 100$] vs λ, the solute diameter (see Table 2) divided by the pore diameter (24.2 nm) (35). The PEO solute diameters, defined as 2 times the hydrodynamic radius, are estimated from tracer diffusion or intrinsic viscosity measurements given in the literature. As expected, the rejection of the 14 kDa sample is small (ca. 15%). The rejection increases with the solute molecular weight, and rejection of the 100 kDa sample is nearly complete (>93%). The solid curve shown in Figure 7 is not a best fit of the data but a prediction without adjustable parameters based on a model by Bungay and Brenner (33, 36) generated using the same procedure detailed in our

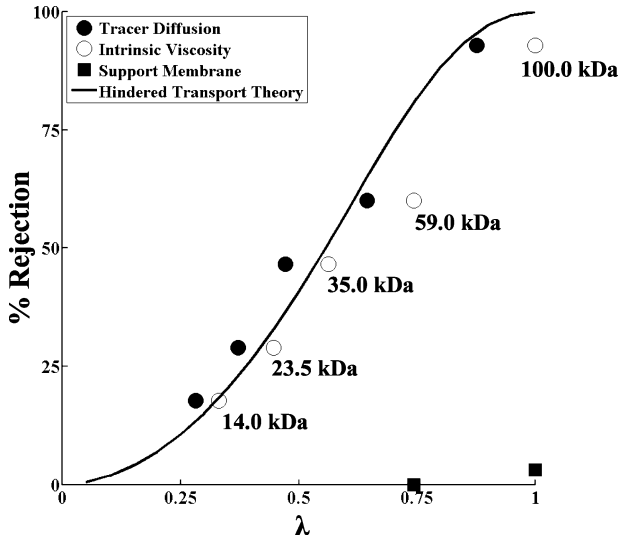

FIGURE 7. Nanoporous PS layer that rejects PEO solutes as expected. Single-solute PEO solutions were used to challenge a composite membrane made using the polymer sample SL(42-15). The resulting rejection curve (filled and open circles) is compared with the predicted curve (solid line) using the hindrance coefficients of Brenner (36) for a 24.2 nm diameter pore. The support membrane alone (filled squares) did not reject a significant percentage of the PEO molecules in this size range.

earlier work (6). The agreement between the experiment and prediction is excellent.

DISCUSSION

Perpendicular Cylinder Formation. In our attempts to produce large areas of membrane, we explored three factors affecting the cylinder orientation in the PS−PLA system. Varying the solvent evaporation rate suggests the perpendicular orientation is a kinetically trapped structure, with the parallel orientation being thermodynamically preferred. This is consistent with the findings of others (24−27). Solvents selective for the majority (i.e., the PS) block lead to perpendicular cylinders, whereas neutral solvents lead to mixed or parallel orientations (24, 27). SEM images show that, above a certain molecular weight, the structure formed after PLA degradation appears as a hexagonally close-packed structure on the surface but resembles pits instead of pores. Similar results were seen in experiments using mixed solvents in the casting solution (37). Finally, as the PLA volume fraction is increased, the cylinders transition from a perpendicular orientation to a parallel orientation under the same casting conditions.

These results suggest a mechanism for perpendicular cylinder formation. When dissolved in the casting solution, the PS−PLA copolymer is not self-assembled because the solvent mediates the unfavorable interactions between the two blocks (38−40). Once the solution is cast onto the microporous support and the solvent begins to evaporate, the solvent concentration at the air−solution interface approaches zero because the atmospheric solvent concentration is zero. While the solvent evaporates, the strength of the unfavorable interactions between the blocks increases until the copolymer reaches the order−disorder transition and microphase separation occurs. We believe that cylinders grow through a nucleation and growth mechanism that begins at the free surface when the solvent evaporates. The copolymer structure that nucleates is probably body-centered-cubic (bcc) spheres. These bcc spheres then fuse epitaxially to form either perpendicular or parallel cylinders, depending on the solvent concentration profile.

Three pieces of experimental evidence discussed below support this mechanism. The phase transitions of block copolymers in the presence of solvents with varying selectivities have been studied extensively (38, 39, 41, 42). We focus on two cases: a neutral solvent and a solvent selective for the majority block. For a neutral solvent, increasing and decreasing the solvent concentration can be pictured as moving up and down a vertical trajectory on the χN vs f_{PLA} morphology map because the solvent swells both blocks equally and dilutes the unfavorable interactions. As the solvent begins to evaporate from a casting solution made using a neutral solvent, the copolymer will phase separate into a cylindrical structure once the order−disorder transition is crossed (38, 41). When the cylinders do precipitate in the absence of some external field, they do so with mixed orientation. The solvent concentration gradient is not strong enough to align the cylinders perpendicularly to the membrane surface. Instead, the cylinders remain a mix of perpendicular and parallel orientations, as seen for films cast from chloroform in Figure 3.

The situation is different for a selective solvent. Now the trajectory follows a diagonal path: the solvent dilutes unfavorable interactions and selectively swells one of the blocks, thereby changing its effective volume fraction (41). Because solvent evaporation causes the order−disorder transition to be reached, bcc spheres form because of the effective composition of the block copolymer. These spheres do not have a preferred direction of growth (i.e., they are zero-dimensional). If the polymer mobility is high when the transition from spheres to cylinders takes place, the cylinders grow along the solvent concentration gradient, forming perpendicular nanostructures. That perpendicular cylinders grow through a spherical intermediate is also supported by the dependence of the orientation on the volume fraction of the PLA block. As the volume fraction of the PLA block increases, the entropic penalty paid to pack the PLA chains into a sphere becomes too great and the polymer transitions directly from a disordered phase to a cylindrical structure.

Potential of PS−PLA as Ultrafilters. The framework presented above for understanding when perpendicular pores form suggests how other copolymer systems can be chosen for UF applications. We note that UF membranes are judged by four performance criteria: selectivity, flux, mechanical integrity, and resistance to fouling. The results in Figure 7 show the superior selectivity of PS−PLA-templated membranes. Like the results for related bicontinuous structures, these results match existing theories for cylindrical pores and give a rejection curve sharper than that for traditional phase-inversion membranes (6).

However, the improved selectivity is compromised currently by relatively low fluxes. All of the pores do not span the selective layer thickness, reducing the flux. The mechanism proposed above implies that coating a thinner selective layer may result in more cylinders spanning the selective layer. Deeper into the film, the driving force for forming perpendicular cylinders decreases, resulting in a mixed perpendicular−parallel cylinder orientation. This transition is observed around 100 nm for the PS−PLA system, suggesting that a selective layer thickness near 100 nm would be a good target. It should be noted that 100 nm is thinner than the selective layer of current composite membranes and may be difficult to achieve. Another technique that could potentially force pores to span the selective layer is to modify the surface energy of the casting substrate. This method has been used successfully by other research groups but for nonporous supports (3, 4).

The poly(ether sulfone) (PES) support, selected because its structure provides the reinforcement required to keep the nanoporous PS intact, may also decrease the flux. The PES support has a low void fraction, possibly blocking a large number of pores in the selective layer. The low fluxes observed are likely a consequence of all of these factors.

Finally, the superior selectivity and higher fluxes promised for these easily fabricated membranes may be lost if the membranes foul easily. There is some reason to expect that they will: the hydrophobic matrix that remains has been shown to foul during surface water treatment (43, 44). At the same time, the overall surface of the membranes is much smoother on a micrometer scale than that of existing UF membranes (10−12), and the potential to modify the surface with PEO brushes exists (1, 2). We look forward to experimentally probing the fouling of these membranes.

Acknowledgment. This work was supported primarily by the MRSEC Program of the National Science Foundation under Awards DMR-0212302 and DMR-0819885.

REFERENCES AND NOTES

(1) Asatekin, A.; Kang, S.; Elimelech, M.; Mayes, A. M. *J. Membr. Sci.* **2007**, *298*, 136–146.
(2) Kang, S.; Asatekin, A.; Mayes, A. M.; Elimelech, M. *J. Membr. Sci.* **2007**, *296*, 42–50.
(3) Yang, S. Y.; Ryu, I.; Kim, H. Y.; Kim, J. K.; Jang, S. K.; Russell, T. P. *Adv. Mater.* **2006**, *18*, 709–712.
(4) Yang, S. Y.; Park, J.; Yoon, J.; Ree, M.; Jang, S. K.; Kim, J. K. *Adv. Funct. Mater.* **2008**, *18*, 1371–1377.
(5) Phillip, W. A.; Rzayev, J.; Hillmyer, M. A.; Cussler, E. L. *J. Membr. Sci.* **2006**, *286*, 144–152.
(6) Phillip, W. A.; Amendt, M.; O'Neill, B.; Chen, L.; Hillmyer, M. A.; Cussler, E. L. *ACS Appl. Mater. Interfaces* **2009**, *1*, 472–480.
(7) Nuxoll, E. E.; Hillmyer, M. A.; Wang, R.; Leighton, C.; Siegel, R. A. *ACS Appl. Mater. Interfaces* **2009**, *1*, 888–893.
(8) Peinemann, K.; Abetz, V.; Simon, P. F. W. *Nat. Mater.* **2007**, *6*, 992–996.
(9) Uehara, H.; Kakiage, M.; Sekiya, M.; Sakuma, D.; Yamonobe, T.; Takano, N.; Barraud, A.; Meurville, E.; Ryser, P. *ACS Nano* **2009**, *3*, 924–932.
(10) Zhu, X.; Elimelech, M. *Environ. Sci. Technol.* **1997**, *31*, 3654–3662.
(11) Elimelech, M.; Zhu, X.; Childress, A. E.; Hong, S. *J. Membr. Sci.* **1997**, *127*, 101–109.
(12) Hoek, E. M. V.; Bhattacharjee, S.; Elimelech, M. *Langmuir* **2003**, *19*, 4836–4847.
(13) Zalusky, A. S.; Olayo-Valles, R.; Wolf, J. H.; Hillmyer, M. A. *J. Am. Chem. Soc.* **2002**, *124*, 12761–12773.
(14) Baker, R. W. *Membrane Technology and Applications*; John Wiley: Chichester, 2004; p 538.
(15) Baker, R. W.; Lokhandwala, K. *Ind. Eng. Chem. Res.* **2008**, *47*, 2109–2121.
(16) Ho, W. S. W.; Sirkar, K. K. *Membrane Handbook*; Kluwer Academic Publishers: Boston, 2001; p 954.
(17) Zalusky, A. S.; Olayo-Valles, R.; Taylor, C. J.; Hillmyer, M. A. *J. Am. Chem. Soc.* **2001**, *123*, 1519–1520.
(18) Olayo-Valles, R.; Guo, S.; Lund, M. S.; Leighton, C.; Hillmyer, M. A. *Macromolecules* **2005**, *38*, 10101–10108.
(19) Vayer, M.; Hillmyer, M. A.; Dirany, M.; Thevenin, G.; Erre, R.; Sinturel, C. *Thin Solid Films* **2010**, in press, corrected proof.
(20) Thurn-Albrecht, T.; Schotter, J.; Kastle, G. A.; Emley, N.; Shibauchi, T.; Krusin-Elbaum, L.; Guarini, K.; Black, C. T.; Tuominen, M. T.; Russell, T. P. *Science (Washington, D.C.)* **2000**, *290*, 2126–2129.
(21) Thurn-Albrecht, T.; DeRouchey, J.; Russell, T. P.; Jaeger, H. M. *Macromolecules* **2000**, *33*, 3250–3253.
(22) Faraone, A.; Magazu, S.; Maisano, G.; Migliardo, P.; Tettamanti, E.; Villari, V. *J. Chem. Phys.* **1999**, *110*, 1801–1806.
(23) Meireles, M.; Bessieres, A.; Rogissart, I.; Aimar, P.; Sanchez, V. *J. Membr. Sci.* **1995**, *103*, 105–115.
(24) Ho, R.; Tseng, W.; Fan, H.; Chiang, Y.; Lin, C.; Ko, B.; Huang, B. *Polymer* **2005**, *46*, 9362–9377.
(25) Kim, S. H.; Misner, M. J.; Xu, T.; Kimura, M.; Russell, T. P. *Adv. Mater.* **2004**, *16*, 226–231.
(26) Kim, S.; Briber, R. M.; Karim, A.; Jones, R. L.; Kim, H. *Macromolecules* **2007**, *40*, 4102–4105.
(27) Kim, G.; Libera, M. *Macromolecules* **1998**, *31*, 2569–2577.
(28) Hansen, C. M. *Hansen Solubility Parameters: A User's Handbook*; CRC Press: Boca Raton, FL, 2000; p 208.
(29) Ryu, D. Y.; Ham, S.; Kim, E.; Jeong, U.; Hawker, C. J.; Russell, T. P. *Macromolecules* **2009**, *42*, 4902–4906.
(30) Cussler, E. L. *Diffusion, Mass Transfer in Fluid Systems*; Cambridge University Press: New York, 2009; p 654.
(31) Bird, R. B.; Stewart, W. E.; Lightfoot, E. N. *Transport Phenomena*; John Wiley: New York, 2002; p 895.
(32) Dullien, F. A. L. *Porous Media: Fluid Transport and Pore Structure*; Academic Press: San Diego, 1992; p 574.
(33) Deen, W. M. *AIChE J.* **1987**, *33*, 1409–1425.
(34) Zeman, L. J.; Zydney, A. L. *Microfiltration and Ultrafiltration: Principles and Applications*; Marcel Dekker: New York, 1996; p 618.
(35) Koppi, K. A.; Tirrell, M.; Bates, F. S.; Almdal, K.; Mortensen, K. *J. Rheol.* **1994**, *38*, 999–1027.
(36) Bungay, P. M.; Brenner, H. *Int. J. Multiphase Flow* **1973**, *1*, 25.
(37) Park, S.; Wang, J.; Kim, B.; Chen, W.; Russell, T. P. *Macromolecules* **2007**, *40*, 9059–9063.
(38) Lodge, T. P.; Hanley, K. J.; Pudil, B.; Alahapperuma, V. *Macromolecules* **2003**, *36*, 816–822.
(39) Lodge, T. P.; Hanley, K. J.; Huang, C.; Ryu, C. Y. *Polym. Mater. Sci. Eng.* **1998**, *79*, 377.
(40) Naughton, J. R.; Matsen, M. W. *Macromolecules* **2002**, *35*, 5688–5696.
(41) Lodge, T. P.; Pudil, B.; Hanley, K. J. *Macromolecules* **2002**, *35*, 4707–4717.
(42) Lodge, T. P.; Blazey, M. A.; Liu, Z.; Hamley, I. W. *Macromol. Chem. Phys.* **1997**, *198*, 983–995.
(43) Bhattacharya, A.; Misra, B. N. *Prog. Polym. Sci.* **2004**, *29*, 767–814.
(44) Maximous, N.; Nakhla, G.; Wan, W. *J. Membr. Sci.* **2009**, *339*, 93–99.

AM900882T